

RSC Advances



This is an *Accepted Manuscript*, which has been through the Royal Society of Chemistry peer review process and has been accepted for publication.

Accepted Manuscripts are published online shortly after acceptance, before technical editing, formatting and proof reading. Using this free service, authors can make their results available to the community, in citable form, before we publish the edited article. This *Accepted Manuscript* will be replaced by the edited, formatted and paginated article as soon as this is available.

You can find more information about *Accepted Manuscripts* in the [Information for Authors](#).

Please note that technical editing may introduce minor changes to the text and/or graphics, which may alter content. The journal's standard [Terms & Conditions](#) and the [Ethical guidelines](#) still apply. In no event shall the Royal Society of Chemistry be held responsible for any errors or omissions in this *Accepted Manuscript* or any consequences arising from the use of any information it contains.



Journal Name

ARTICLE

Water-dispersible Polyphosphate Grafted Fe₃O₄ Nanomagnets for Cancer Therapy

Jerina Majeed^a, K. C. Barick^{a*}, Neena G. Shetake^b, B. N. Pandey^b, P. A. Hassan^{a*}, A. K. Tyagi^{a*}

Received 00th January 20xx,
Accepted 00th January 20xx

DOI: 10.1039/x0xx00000x

www.rsc.org/

We report the development of a new class of water-dispersible polyphosphate grafted Fe₃O₄ nanomagnets (PPNM) by a facile soft-chemical approach. The grafting of polyphosphate with Fe₃O₄ nanoparticles was evident from Fourier transform infrared (FTIR) spectroscopy, thermogravimetric analysis (TGA), dynamic light scattering (DLS) and zeta-potential measurements. X-ray diffraction (XRD) and transmission electron microscopy (TEM) analyses reveal the formation of highly crystalline Fe₃O₄ nanoparticles with average size of about 10 nm. These nanoparticles show good colloidal stability, strong magnetic field responsiveness and protein resistance characteristics. The induction heating studies confirmed localized heating of these superparamagnetic PPNM with good intrinsic loss power under AC magnetic field (AMF). The drug loading and release behavior of PPNM was explored using doxorubicin hydrochloride (DOX) as a model drug. The decrease of fluorescence intensity and surface charge of drug loaded PPNM strongly suggest the conjugation of DOX with PPNM. The cell viability and hemolysis assays suggest that PPNM do not have adverse toxic effects for further *in-vivo* use. Specifically, high loading affinity for DOX with their sustained release, substantial cellular internalization and self-heating capacity makes these novel magnetic nanoparticles suitable for drug delivery and hyperthermia therapy applications.

Introduction

Over the last few decades, significant attention is focused on magnetic nanoparticles (MNP) as potential tool for various biomedical applications such as drug delivery, magnetic hyperthermia and magnetic resonance imaging (MRI).¹⁻⁵ In particular, Fe₃O₄ nanoparticles have received extensive attention due to their unique properties like superparamagnetism and low toxicity. Practical *in-vivo* usage of these particles requires size below 100 nm as well as their colloidal stability and biocompatibility in the physiological medium. However, the bare Fe₃O₄ nanoparticles prepared by co-precipitation method even though have an average size of 10 nm, they are polydispersed, and tend to aggregate and adsorb proteins quickly in water or physiological media.⁶ In addition, for most of the biomedical applications, the significant challenge is to avoid unwanted uptake of MNP by the reticuloendothelial system (RES). In order to overcome the above drawbacks, Fe₃O₄ nanoparticles are often surface engineered by coating with various biocompatible, stimuli responsive organic and inorganic functional molecules.⁷⁻¹⁴ These coating molecules not only stabilize nanoparticles but also provide terminal functional groups that can be utilized for attaching targeting moieties as well as drugs. Further, the use of such stimuli-responsive nanoparticles in cancer therapy can increase drug accumulation at target site, decrease toxicity and avoid under- or over-dosing.^{15,16}

In general, the stability of the bonding between functional molecules and Fe₃O₄ nanoparticles is crucial for biomedical applications. The main drawback of the surface engineered MNP currently in use is that the polymer coatings are not covalently

bound to the MNP surface and will easily be detached. Moreover, the polymer coatings further cause a significant increase in the overall hydrodynamic diameter of the particles and thereby affecting their bio-distribution as well as clearance. Thus, further functionalization with targeting ligands increases the complexity. The polymer shell around the MNP core influences the magnetic relaxivity dramatically.¹⁷ Therefore, the covalent attachment of nonpolymeric layers that would improve the stability of MNP under physiological conditions without affecting particle size drastically or undermining magnetic properties (e.g., relaxivity and saturation magnetization) while still providing sites for attaching targeting ligands (e.g., antibodies) would be useful. Thus, there is an emergent interest in developing biocompatible magnetic nanocarriers with suitable surface functionality for biomedical applications.

Recent work with organosilanes, carboxylate and phosphonate anchored layers grafted on MNP are proven to be better anchoring groups without adversely affecting their properties. Yee et al. reported the binding of alkane phosphonic acids onto the surface of ferric oxide particles either by one or both oxygen atoms of phosphonate group.¹⁸ Sahoo et al. demonstrated the conjugation of alkyl phosphonates and phosphate to Fe₃O₄ nanoparticles via formation of P-O-Fe bonding.¹¹ Recently, our research group reported the preparation of water-dispersible and biocompatible Fe₃O₄ nanoparticles using sodium hexametaphosphate (cyclic phosphate molecule) as surface passivating agent.¹⁹ The formation of these water dispersible Fe₃O₄ nanoparticles has been attributed to the presence of bioactive phosphate molecules on their surface. This work further propelled us to investigate the use of linear phosphate molecule in stabilization of Fe₃O₄ nanoparticles. Other research groups also reported the strong interaction between inorganic core and the phosphonic moiety and the most interesting moiety seems to be triphosphate, a class of polyphosphates.^{11,18-21} The Food and Drug Administration (FDA) approved sodium tripolyphosphate (STPP) is widely used as a preservative for food and also as a polyanion cross-linker in polysaccharide based drug

^aChemistry Division, Bhabha Atomic Research Centre, Mumbai – 400 085, India, E-mail: kbarick@barc.gov.in, hassan@barc.gov.in, aktyagi@barc.gov.in, Fax: + 91 22 2550 5151, Tel: + 91 22 2559 0284.

^bRadiation Biology and Health Sciences Division, Bhabha Atomic Research Centre, Mumbai – 400 085, India.

†Electronic Supplementary Information (ESI) available: TEM images, SAED pattern, FTIR, TGA, DLS, UV-visible, zeta-potential and magnetization plots, and protein-particle interaction data (Fig. S1-S10, Table S1). See DOI: 10.1039/b000000x/

delivery systems.²² The chitosan/ tripolyphosphate nanoparticles (CS/ TPP) have been used as an alternative to chitosan to encapsulate peptides, proteins, pDNA and siRNA²³⁻²⁵. In a review article, Rao et al. have demonstrated the essential roles of polyphosphates in the virulence of major diseases, such as dysentery, tuberculosis, and anthrax, as well as in apoptosis, in the proliferative aspects of cancer, in osteoporosis, and in aging.²⁶ These polyphosphates are hydrolyzed into simpler phosphates, which in moderate amounts are nutritious. Being a linear molecule, tripolyphosphate has higher affinity for metal ions. It binds strongly to metal cations as both a bidentate and tridentate chelating agent. Even though, STPP is extensively used in preparation and stabilization of chitosan nanoparticles, its use as a coating material in preparation of aqueous-stable Fe₃O₄ nanoparticles is hardly reported.

Herein, we report preparation of polyphosphate grafted Fe₃O₄ nanomagnets (PPNM) for drug delivery and hyperthermia treatment of cancer. It has been observed that the use of tripolyphosphate as surface passivating agent provides excellent biocompatibility and colloidal stability to particles. PPNM showed good magnetic field responsivity and excellent self-heating efficacy under AC magnetic field (AMF), which is essential for their hyperthermia application. Further, high affinity of these nanoparticles towards positively charged DOX, and their pH triggered release and substantial cellular internalization makes them suitable for drug delivery. This study may permit the design of novel combinatorial therapy in which the synergy between the nanoparticle hyperthermia and chemotherapeutic agents can provide effective treatment with minimal side effects.

Experimental

Materials

Ferrous chloride tetrahydrate (FeCl₂·4H₂O), ferric chloride hexahydrate (FeCl₃·6H₂O), 3-(4,5-dimethyl-2-thiazolyl)-2,5-diphenyl-2H-tetrazolium bromide (MTT), doxorubicin hydrochloride (DOX) and bovine serum albumin (BSA) were purchased from Sigma-Aldrich. Dulbecco's modified Eagle medium (DMEM) and fetal calf serum (FCS) were obtained from Invitrogen, USA and Himedia Laboratories, India, respectively. Ammonia (25%) and dimethyl sulfoxide (DMSO) were procured from Thomas Baker Chemical Pvt. Ltd., India and SD Fine Chemicals, India, respectively. Sodium tripolyphosphate was purchased from SRL Pvt. Ltd., India. All chemicals are of analytical grade and used without further purification. The acetate buffer (AB) pH 4 and 5, and phosphate buffered saline (PBS)-pH 7.4 were prepared using standard protocols.

Synthesis of polyphosphate grafted Fe₃O₄ nanomagnets

Polyphosphate grafted Fe₃O₄ nanomagnets (PPNM) were prepared by one pot co-precipitation of Fe²⁺ and Fe³⁺ ions in basic medium. In brief, FeCl₂·4H₂O (1.988 g) and FeCl₃·6H₂O (5.406 g) were dissolved in 80 ml of water in a round bottom flask and temperature was slowly increased to 70 °C in nitrogen atmosphere under constant mechanical stirring at 1000 rpm. The temperature was maintained at 70 °C for 30 min and then 30 ml of ammonia solution (25 %) was added instantaneously to the above reaction mixture, and kept under stirring for another 30 min at the same temperature. Then, 10 ml aqueous solution (0.2 gm/ml) of sodium tripolyphosphate was added and temperature was slowly raised to 90 °C, and reacted

for 60 min under stirring. The obtained precipitates were then thoroughly rinsed with water and separated from the supernatant solution by using a permanent magnet. For comparative purpose, bare Fe₃O₄ MNP were prepared in similar method without using polyphosphate as coating material.

Characterizations

X-ray diffraction (XRD) patterns were recorded on a Philips powder diffractometer PW3040/60 with Cu K α radiation. The crystallite sizes are estimated from the X-ray line broadening using Scherrer formula. The infrared spectra were recorded in the range 4000-400 cm⁻¹ on a Fourier Transform Infrared Spectrometer (FTIR, Bomem, MB series). The transmission electron micrographs were taken by Philips CM 200 TEM. Thermal analysis of samples was performed under argon atmosphere with a scanning rate of 10 °C/min using TGA, Setaram Instrumentation. DLS measurement was performed using a Malvern 4800 Autosizer employing a 7132 digital correlator for the determination of hydrodynamic diameter. The zeta-potential measurements were done by Zetasizer nano series, Malvern Instruments. The colloidal stability assay was investigated by measuring the absorbance at wavelength of 350 nm for different time intervals using JASCO V-650, UV-visible spectrophotometer. The field dependent magnetization and zero field cooled-field cooled (ZFC-FC, at an applied field of 100 Oe) measurements were carried out by Physical Property Measurement System (PPMS, Quantum Design). The concentration of phosphorus in sample was measured using an inductively coupled plasma-optical emission spectrometer (ICP-OES, Activa, Horiba Jobin Yvon).

The heating ability of PPNM suspension was obtained from the time-dependent calorimetric measurements using an induction heating unit (Easy Heat 8310, Ambrell). 1 ml of aqueous suspension PPNM of desired concentration was taken in an eppendorf tube with suitable arrangements to minimize the heat loss. The AMF of 0.251, 0.293 and 0.335 kOe at a fixed frequency of 265 kHz were used to evaluate the specific absorption rate (SAR). The SAR was calculated using the following equation²⁷:

$$SAR = C \frac{\Delta T}{\Delta t} \frac{1}{m_{Fe}}$$

where, C is the specific heat of solvent ($C = C_{water} = 4.18 \text{ J/g } ^\circ\text{C}$), $\Delta T/\Delta t$ is the initial slope of the time-dependent temperature curve and m_{Fe} is mass fraction of Fe₃O₄ in the sample. The rise in temperature was also monitored using a high resolution infrared (IR) camera (Thermal Imager Testo 875-1), and analyzed by a thermography software (Testo IR Soft Software, version 3.1). The concentration of Fe in PPNM suspension was obtained by phenanthroline spectrophotometric method.²⁸

The anticancer agent, DOX was used as a model drug to estimate the drug loading and release behavior of the PPNM. In order to investigate the interaction of DOX with PPNM, we have performed zeta-potential and fluorescence spectroscopic studies. The aqueous dispersion of different amounts of PPNM (0, 20, 40, 60, 80, 100, 120 and 140 μg) were added to a 1 ml of DOX solution (10 $\mu\text{g}/\text{ml}$) and mixed thoroughly by shaking at room temperature for 15 min. The fluorescence spectra of the supernatant (obtained after magnetic sedimentation of DOX loaded PPNM) were then recorded using Hitachi F 2500 fluorescence spectrophotometer. The fluorescence intensities of supernatants (washed drug molecules were also taken into consideration for calculations) against that of pure DOX solution were used to determine the loading efficiency. The

encapsulation efficiency (w/w %) was calculated using the following relation:

$$\text{Encapsulation efficiency (\%)} = \frac{I_{\text{DOX}} - I_s - I_w}{I_{\text{DOX}}} \times 100$$

where, I_{DOX} is the fluorescence intensity of pure DOX solution, I_s the fluorescence intensity of supernatant and I_w the fluorescence intensity of washed DOX (physically adsorbed DOX molecules). The drug loading content was determined as follows:

$$\text{Loading content (\%)} = \frac{\text{Weight of encapsulated DOX}}{\text{Weight of PPNM}} \times 100$$

For release study, we have quantified the amount of DOX-PPNM according to the loading efficiency. The loading was carried out, at increased scale, by incubating 0.5 ml of aqueous solution of DOX (1 mg/ml) with 1 ml of the aqueous suspension (pH ~ 7.5) of PPNM (5 mg/ml) for 1 h in dark (however, no decrease in fluorescence intensities was observed after 15 min of interaction). Drug loaded samples were separated from the free-standing drug molecules through magnetic separation and carefully washed by milli Q water. The pH-triggered drug release studies were carried out under reservoir (r)-sink (s) conditions. The drug-loaded PPNM (5 mg) were immersed into 5 ml of respective release medium (AB-pH 4, AB-pH 5) and then put into a dialysis bag. The dialysis was performed against 200 ml of PBS-pH 7.4 under continuous stirring at 37 °C to mimic the cellular environment. 1 ml of the external medium was withdrawn and replaced with fresh PBS at fixed interval of times to maintain the sink conditions. The amount of DOX released was determined by measuring the fluorescence emission at 585 nm (excitation wavelength: 490 nm) using a plate reader (Infinite M1000, Tecan-I control, Switzerland) against the standard plot prepared under similar conditions. Each experiment was performed in triplicates and standard deviation was given in the plot.

The biocompatibility of PPNM to mouse skin fibrosarcoma (WEHI-164) cell line was investigated by MTT assay. Cells (0.25×10^6) were seeded overnight in petridishes (P-60) containing 4 ml Dulbecco's Modified Eagle Medium (DMEM) supplemented with 10% fetal calf serum (FCS) and antibiotics (100 U ml⁻¹ penicillin and 100 µg ml⁻¹ streptomycin) in a humidified atmosphere of 5% CO₂ at 37 °C. Then different concentrations of PPNM were added to cells and incubated for another 48 h in culture conditions. Then, the media containing PPNM was carefully removed and the cells were further incubated with 0.5 ml of MTT solution (0.5 mg/ml) in culture conditions for 2 h. The supernatant was aspirated and 1 ml of DMSO was added to each culture dish to solubilize the MTT crystals. The crystals were thoroughly dissolved and further diluted with DMSO (1: 10). 200 µl of above solution from P-60 culture dishes was transferred to 96 well plates and the absorbance was measured in a microplate reader (Tecan infinite 200 PRO, Switzerland) at 544 nm. The cell viability was calculated by comparing the absorption of treated cells to that of control, which was defined as 100%.

Cellular uptake of DOX loaded PPNM was studied by confocal laser scanning microscopy (CLSM) using WEHI-164 cell line. For CLSM imaging, cells (0.5×10^6) were seeded on glass coverslips and cultured overnight. The cells were then treated with DOX-PPNM (0.5 µM DOX) for 3 h under culture conditions, followed by washing with PBS. The cells were mounted on a glass slide in cell mounting medium (Invitrogen, USA) containing DAPI for nuclear staining. These cells were then imaged by CLSM (LS510 Meta, Carl Zeiss, Germany). The excitation source used was an Ar ion laser (488 nm for DOX and 364 nm for DAPI) and the emission window was set at 575–615 nm and 430–480 nm for DOX and DAPI, respectively.

The protein-particle interaction and hemolysis assay studies were performed to evaluate the protein resistance characteristics (with BSA) and hemocompatibility (with human whole blood) of PPNM, respectively as reported elsewhere.^{2,27}

Results and discussion

Fig. 1 shows (a) XRD patterns of bare MNP and PPNM, and (b) TEM image of PPNM (inset shows its HRTEM image). XRD pattern shows the formation of a single-phase cubic inverse spinel Fe₃O₄ structure with lattice constant, $a = 8.378 \text{ \AA}$, which is very close to the reported value of magnetite (JCPDS Card No. 88-0315, $a = 8.375 \text{ \AA}$). The presence of sharp and intense diffraction peaks confirmed the formation of highly crystalline particles. The average crystallite sizes were found to be around 10 nm from X-ray line broadening. These sizes are comparable to the results obtained from TEM. The TEM image of PPNM clearly shows the formation of almost spherical nanoparticles of size about 10 nm. It could be clearly seen that these PPNM have a good distribution, with a lower percentage of agglomeration with respect to bare MNP (TEM image of bare MNP is shown in Fig. S1, †ESI). From HRTEM image of PPNM (inset of Fig. 1b), the average lattice spacing (d_{hkl}) was measured to be ~0.30 nm which corresponds to (220) plane of inverse spinel Fe₃O₄.²⁹ Furthermore, the selected area electron diffraction (SAED) pattern of bare MNP and PPNM can be indexed to highly crystalline reflections, such as (220), (311), (400), (422), (511) and (440) of cubic inverse spinel Fe₃O₄ structure, which is consistent with the XRD result (a typical SAED pattern of PPNM shown in Fig. S2, †ESI).

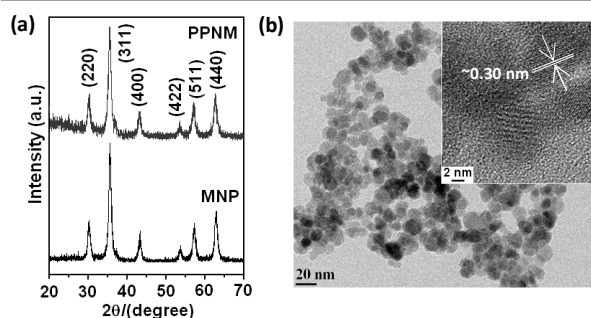


Fig. 1. (a) XRD patterns of bare MNP and PPNM, and (b) TEM image of PPNM (inset of Fig. 1b shows the HRTEM image of PPNM).

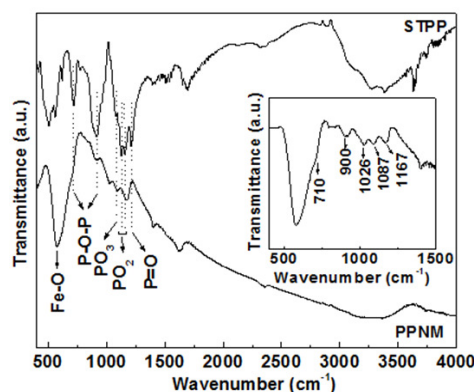


Fig. 2. FTIR spectra of STPP and PPNM with their peaks assignments (inset shows expanded FTIR spectrum of PPNM in the range of 400 – 1500 cm⁻¹).

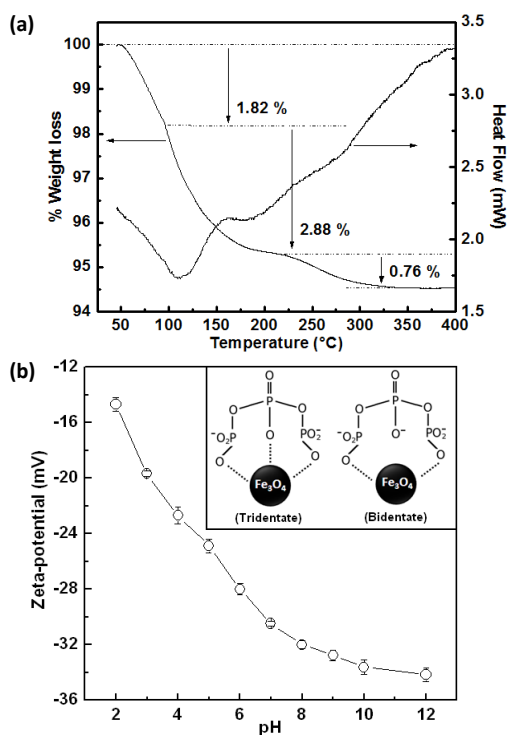


Fig. 3. (a) TGA-DTA and (b) pH dependent zeta-potential plots of PPNM (inset of Fig. 3b shows the possible schematic representation for chemical conjugation of STPP onto the surface of Fe_3O_4 nanoparticles).

FTIR spectroscopy is a useful tool to identify the functional groups present on the surface of nanoparticles. In the present case, it is applied to find out whether there are any vibrational bands owing to the presence of phosphate group on the surface of MNP. FTIR spectra of STPP and PPNM along with their peak assignments are shown in Fig. 2. It has been observed that the IR bands for STPP are well resolved, while those of the PPNM are rather broad and less intense. In the spectrum of STPP, the characteristic bands attributed to phosphates vibrations are appeared at 1215 cm^{-1} (P=O stretching), 1160 and 1130 cm^{-1} (asymmetric and symmetric stretching vibrations in PO_2 group), 1078 cm^{-1} (asymmetric and symmetric stretching vibrations in PO_3 group), and 918 and 715 cm^{-1} (asymmetric and symmetric stretching of the P-O-P bridge).³⁰ These bands were absent in the spectrum of bare Fe_3O_4 MNP (Fig. S3, †ESI), whereas they appeared in the spectrum of PPNM with slight shifting of band position in the range of 700 to 1250 cm^{-1} with band at 710 , 900 , 1026 , 1087 and 1167 cm^{-1} . Further, the intense peak at around 575 cm^{-1} in PPNM can be attributed to the Fe-O stretching vibrational mode of Fe_3O_4 .²⁷

Fig. 3 shows (a) TGA-DTA and (b) pH dependent zeta-potential plots of PPNM. The TGA analysis of PPNM showed a total weight loss of 5.46% upto $400\text{ }^\circ\text{C}$ (Fig. 3a), whereas that of bare Fe_3O_4 MNP was 2.5% (Fig. S4, †ESI). The higher weight loss for PPNM further confirmed the presence of organic molecules on the surface of Fe_3O_4 nanoparticles. Furthermore, TGA plot of PPNM revealed a three-step thermal decomposition profile for PPNM. An initial weight loss of about 1.82% with an endothermic peak at $\sim 110\text{ }^\circ\text{C}$ is associated with the removal of residual water, and physically absorbed hydroxyl and STPP from surface of MNP. The second and third step weight losses (3.64%) were observed due to

decomposition of polyphosphate moieties present on the surface. These two stages weight loss with endothermic shoulder at about 180 and $275\text{ }^\circ\text{C}$ may be attributed to either bilayer coating of STPP or chemical conjugation phosphate molecules onto the surface of Fe_3O_4 particles by two different forms. The bilayer coating of STPP can be ruled out as the introduction of second layer of phosphate polyanion is not electrostatically favorable onto the negatively charged PPNM. Thus, it is assumed that polyphosphate molecules of STPP were conjugated to the surface of Fe_3O_4 nanoparticles by two different forms chemical bonding between oxygen atoms of polyphosphate and Fe_3O_4 .¹⁸ In one case, the polyphosphate moiety is bonded through its three oxygen atoms, resulting in a stronger bridging geometry (tridentate) and a higher desorption temperature. In the second case, only two oxygen atoms participate in the bonding (bidentate), resulting in weaker bonding and a lower desorption temperature. From ICP-OES analysis, the amount of STPP molecules present on the surface of PPNM was found to be 126 mg/g of particles.

After the successful functionalization of polyphosphate moieties onto the surface of nano-magnets, it is important to check the colloidal stability for their practical applications. The colloidal stability of the PPNM was assessed from the changes in light scattering intensity as well as extinction changes with time. DLS measurement indicates that these particles render aqueous colloidal dispersion with mean hydrodynamic diameter of 43 nm (Fig. S5, †ESI). The higher value of hydrodynamic diameter observed by DLS, as compared to TEM arises from the presence of hydrated organic moiety and the inherent polydispersity in the distribution.^{31,32} However, the light scattering intensity and polydispersity index hardly varies with time revealing their good aqueous colloidal stability. Further, the insignificant change in absorbance of PPNM suspension in aqueous media even up to 72 h indicates their good colloidal stability (Fig. S6, †ESI). These nanoparticles are hydrophilic in nature due to the hydrogen bonding association of surface functional groups and water.

Electrostatic contribution to the stabilization of particle is evident from zeta-potential measurements. The variation in the zeta-potential of PPNM suspensions with varying pH values (0.05 mg/ml) are depicted in Fig. 3b. From zeta-potential measurements, no isoelectric point (pH of zero-point charge) was observed for PPNM in the pH range of 2 - 12 , whereas that of bare Fe_3O_4 was 6.67 (Fig. S7, †ESI). Moreover, the high negative surface charge of PPNM (at $\text{pH}>4$) makes them colloidal stable in aqueous phase. The high negative charge on these particles arises from the grafting of phosphate groups on MNP. In addition, the electrostatic repulsive force originating from the ionization of the phosphate groups provides additional stability to the particles. Furthermore, the high negative zeta-potential of PPNM at physiological medium (-30 mV) could decrease the possibility of their combination with hemoglobin, which would play a significant role in improving the stability and blood compatibility. Based on the TGA and zeta-potential measurements, the possible schematic representation for chemical conjugation of STPP onto the surface of Fe_3O_4 nanoparticles is shown in inset of Fig. 3b.

In order to assess the potential of PPNM in targeted drug delivery and hyperthermia, further studies were performed on their magnetic and thermo-magnetic properties. The field-dependent magnetization plots of PPNM at 5 and 300 K are shown in Fig. 4. These PPNM exhibit superparamagnetic behavior without magnetic hysteresis and remanence at 300 K , whereas ferrimagnetic behavior with a coercivity of about 80 Oe and a remanence of 11.8 emu/g is observed at 5 K . The appearance of hysteresis at lower temperature

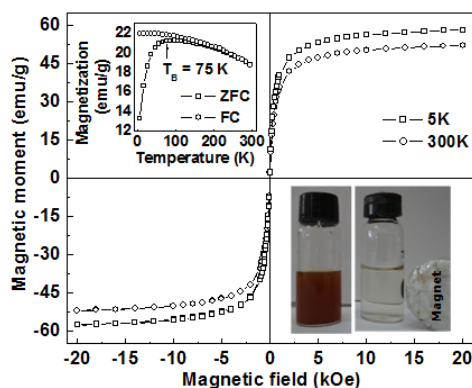


Fig. 4. Field dependent magnetization plots of PPNM at 5 and 300 K (top inset shows ZFC-FC plots of PPNM at an applied field of 400 Oe bottom and bottom inset shows photographs of PPNM suspension in presence and absence of permanent magnet of field strength ~ 2.5 kOe).

points to the magnetic ordering of sample at lower temperature. This transition from superparamagnetic behavior to ferro/ferrimagnetic behavior below the particular temperature, i.e., blocking temperature (T_B) is usually observed in MNP.³³ The ZFC-FC plot (top inset of Fig. 4) shows that the blocking temperature (T_B) of the PPNM is 75 K at an applied field of 400 Oe. The magnetization values of PPNM were found to be 58.2 and 52.2 emu/g, at 20 kOe for 5 and 300 K, respectively. Further, the bare Fe_3O_4 prepared by similar route gave a magnetization of 67.6 emu/g at 300 K (Fig. S8, †ESI). The magnetization of PPNM is reduced by $\sim 22\%$ as compared to the bare Fe_3O_4 , although TGA showed only about 5.46 % weight loss. The magnetization of bare MNP could be possibly arising from the clustering behavior of the uncapped MNP, which will contribute to the increase in magnetization due to the exchange coupling and dipolar interaction among the surface ions.³⁴ Whereas in the case of PPNM the presence of bulkier non-magnetic polyphosphate group on the surface will suppress the contribution from exchange coupling as well as dipolar interactions among particles. However, the retention of superparamagnetic properties at room temperature with good magnetic field responsivity (bottom inset of Fig. 4) makes these nanoparticles suitable for hyperthermia and drug delivery applications.

The effect of magnetic field strength and concentration of particle on heating ability of PPNM were evaluated. Fig. 5 shows the temperature vs. time plots of (a) 2.3 mg/ml of Fe at different applied fields and (b) different concentrations of Fe at an applied field of 0.335 kOe. The temperature vs. time plots of PPNM suspension showed a time-dependent gradual increase in temperature under applied AMF. It has been observed that a magnetic field of 0.251 kOe at fixed frequency of 265 kHz was enough for raising the temperature of the magnetic suspension of 2.3 mg/ml to 42–43 °C (hyperthermia temperature) within 20 min. At this temperature, various cellular damaging mechanisms such as apoptosis, protein denaturation and DNA cross-linking may occur to destroy the cancer cells.^{35,36} Further, the required hyperthermia temperature was achieved much faster with increasing field strength, which is apparent as the heat generation/dissipation (P) is proportional to the square of applied AC magnetic field (inset of Fig. 4a) as follows²⁷:

$$P = \pi \mu_0 \chi_0 H^2 f \frac{2\pi f \tau_{eff}}{1 + (2\pi f \tau_{eff})^2}$$

where, μ_0 is the permeability of free space, χ_0 is the magnetic susceptibility, H is the magnetic field amplitude, f is the frequency and τ_{eff} is the effective relaxation time. In heating of superparamagnetic Fe_3O_4 nanoparticles under AMF, a rise in temperature is mainly associated with the combined effect of Néel and Brownian relaxation losses.^{27,37} The Néel and Brownian relaxation losses are associated with the magnetic moment rotations within the particles and with the entire particles, respectively. The relaxation times are given by the following equations:

$$\tau_N = \tau_0 e^{KV_M/k_B T}$$

$$\tau_B = \frac{4\pi\eta R_H^3}{k_B T}$$

$$\tau_{eff} = \frac{\tau_N \tau_B}{\tau_N + \tau_B}$$

where, τ_B is Brownian relaxation time, τ_N is Néel relaxation time, $\tau_0 \approx 10^{-9}$ s, K is anisotropy constant, V_M is volume of the Fe_3O_4 nanoparticles, k_B is Boltzmann's constant, T is temperature, η is viscosity and R_H is hydrodynamic particle radius. Since the aqueous suspension of Fe_3O_4 nanoparticles is semiconducting in nature with high resistivity ($\rho = 10^2$ Ohm-cm), heat-generation under AMF will be negligible from eddy current loss.³⁸ Further, heat-generation due to hysteresis loss will be negligible for superparamagnetic nanoparticles (as particle size is less than the critical diameter/single domain).³⁸

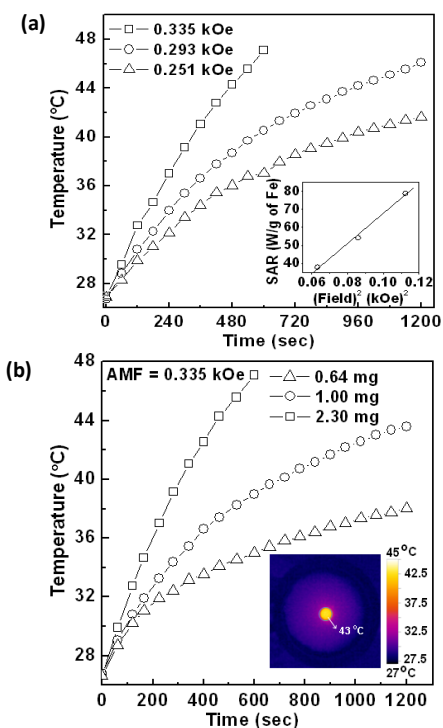


Fig. 5. Temperature vs. time plots of (a) 2.3 mg/ml of Fe at different applied fields (inset shows the linear relationship between SAR and applied AMF) and (b) different concentrations of Fe at an applied field of 0.335 kOe (inset shows the IR thermogram of 1 mg/ml of Fe at AMF of 0.335 kOe).

The use of Fe₃O₄ nanoparticles in hyperthermia therapy depends on their heating ability, which is expressed in terms of the specific absorption rate (SAR). The SAR values of PPNM were found to be 38, 54.3 and 74.0 W/g of Fe with an applied field of 0.251, 0.293 and 0.335 kOe, respectively. Since SAR values are dependent on the used field strength and frequency, we have calculated system-independent intrinsic loss power (ILP) as follows³⁹:

$$ILP = \frac{SAR}{H^2 f}$$

where, H is the field strength and f is the frequency. The ILP values obtained were 0.35, 0.37 and 0.39 nHm²/kg with an applied field of 0.251, 0.293 and 0.335 kOe, respectively for 2.30 mg/ml of the sample, which itself shows the normalization ineffective of the different applied field. Further, the rise in temperature is also found to be dependent on the concentration of particles in the suspension. However, the heating efficacy (i.e., SAR) decreases with increasing Fe concentration (even though time required for reaching hyperthermia temperature decreases). This may be due to the decrease in Brownian contribution to hyperthermia and increase in magnetic dipole-dipole interactions between nanoparticles in suspension as a result of the increase in local concentration.⁴⁰ The ILP values obtained in present study are in the range of those reported for commercially available ferrofluids.³⁹ The rise in temperature of PPNM suspension under AMF is also visualized from IR thermogram (centre bright circle) and it further demonstrates the localized heating of PPNM (inset of Fig. 5b). This is highly advantageous for the *in-vitro* hyperthermia. Therefore, these PPNM can be used as excellent heating source for hyperthermia treatment of cancer.

The negatively charged surfaces of PPNM make it an attractive vehicle for delivery of electrostatically bound drug molecules. DOX a cationic drug used in chemotherapy is chosen as a model drug to estimate the drug loading and release behavior of PPNM. The high affinity of DOX for negatively charged species are well reported in literatures.^{2,40-43} We have performed zeta-potential and fluorescence spectroscopic studies to explore the binding of DOX with PPNM. The zeta-potential of 1 ml aqueous suspension of PPNM (100 µg) is increased from -32.0 mV to -9.5 mV upon interacting with 10 µg of DOX (Fig. S9, †ESI). This change in surface charge value can be attributed to the binding of cationic DOX with negatively charged nanomagnets through electrostatic interactions,

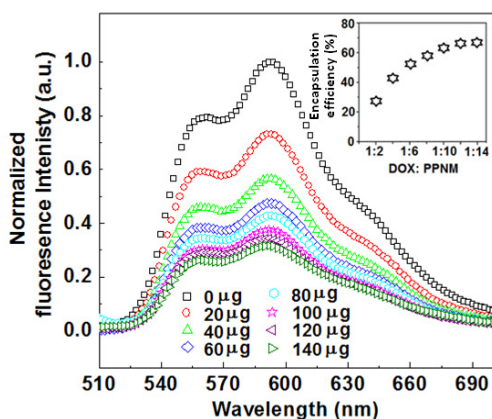


Fig. 6. Normalized fluorescence spectra of 1 ml of DOX (10 µg) upon reacted with different amounts (0, 20, 40, 60, 80, 100, 120 and 140 µg) of PPNM. Inset shows the encapsulation efficiency obtained from decrease in fluorescence intensities.

thus partially passivating the surface. The interaction of DOX molecules with PPNM was also apparent from the variation in fluorescence intensity of the supernatant liquid after removal of DOX loaded PPNM through magnetic separation (Fig. 6). The fluorescence intensity of supernatant liquid drops with increasing concentration of PPNM, due to increase in available surface site for drug conjugation. From encapsulation efficiency plot (inset of Fig. 6), the encapsulation efficiency is found to be strongly dependent on the weight ratio of PPNM to DOX (no significant increase in encapsulation efficiency is observed beyond 1:14 ratio). An encapsulation efficiency (w/w) of 64 % was obtained upon interacting 0.5 ml of aqueous solution of DOX (1 mg/ml) with 2.5 ml of the aqueous suspension of PPNM (5 mg) for 1 h in dark. Further, the drug loaded PPNM offered a DOX loading content of 6.4 %. It is worth mentioning that PPNM still reserve water solubility and good dispersibility after being coupled with DOX molecules (TEM image of DOX loaded PPNM is shown in Fig. S10, †ESI).

The release of drug from DOX-PPNM system (Fig. 7) shows a time dependent release of drug molecules and release rate increased with decreasing pH value. The initial stage of drug release is characterized by a rapid release of drug, followed by a slow and steady release of drug. It has been noted that about 54.6 and 60.5 % of loaded DOX molecules were released from the DOX-PPNM at pH 5 vs. pH 7.4 and pH 4 vs. pH 7.4, respectively after 48 h under reservoir-sink conditions at 37 °C (Fig. 7). The release of DOX could be attributed to the weakening of the electrostatic interactions between cationic DOX and partially neutralized phosphate groups on the surface of nano-magnets at acidic pH. Thus, the pH-triggered DOX release occurs across the range of pH values usually found in intracellular matrix (pH~4), or the local environment in some cancerous tissues, thereby enabling targeted therapeutics by passive release at the clinically relevant sites.

In-vitro experiments were also conducted to determine the effects of these PPNM on cell viability. From MTT assay, it has been observed that PPNM had negligible effect on the viability of WEHI-164 cells even at concentrations as high as 1.5 mg/ml (Fig. 8a). This result indicates that PPNM have minimal inherent toxicity on WEHI-164 cells. However, DOX and DOX-PPNM showed significant reduction in proliferation of WEHI-164 cells (Fig. 8b). The relatively low cytotoxicity of DOX-PPNM, compared to pure DOX, can be ascribed to the sustained release behavior of the drug from DOX-PPNM system (the loaded drug is expected to release slowly over experimental period⁴⁴). In addition, the percentage of hemolysis was found to be around 3% upon incubation of 0.5 mg of PPNM, which indicates their good hemocompatibility. We also investigated

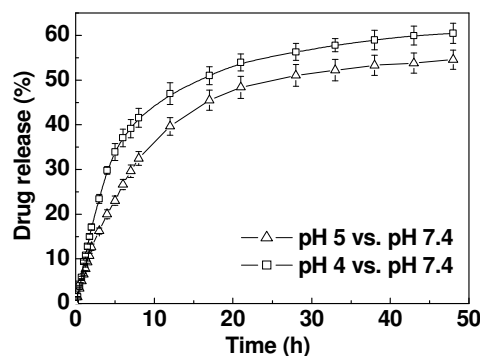


Fig. 7. pH dependent drug release profile of DOX-PPNM in cell mimicking environment (reservoir (r): pH 5/pH 4 and sink (s): pH 7.4) at 37 °C.

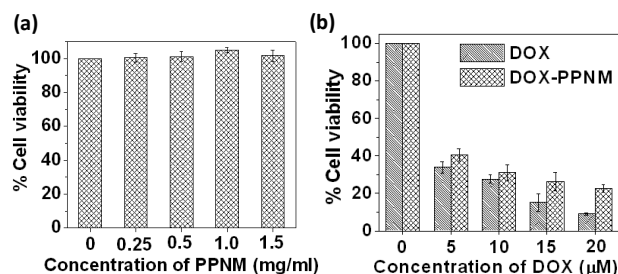


Fig. 8. Viabilities of WEHI-164 cells incubated in medium containing difference concentrations of (a) PPNM and (b) DOX and DOX-PPNM at 37 °C for 48 h.

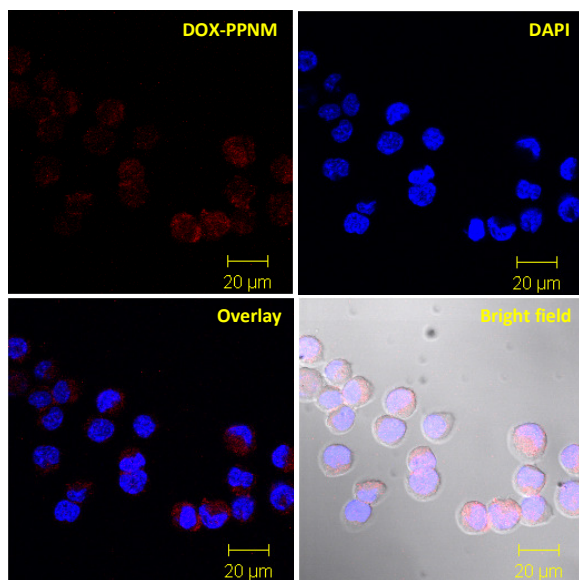


Fig. 9. CLSM images of WEHI-164 cells after incubation with the DOX-PPMN and DAPI at culture conditions.

the interaction of PPNM with BSA protein in physiological medium (0.01 M PBS, pH 7.4). The PPNM do not show any significant change in the zeta-potential (Table S1, ESI[†]) even after incubation with BSA for 2 h, revealing their protein resistance characteristics in physiological medium.

The high loading affinity of PPNM for DOX and their sustained release, and cytotoxicity effect further impelled us to explore the cellular uptake of DOX-PPNM. Fig. 9 shows the CLSM images of WEHI-164 cells after incubation with DOX-PPMN under culture conditions. A significant uptake of DOX-PPMN was clearly observed from the red fluorescence image arising from DOX emissions, suggesting that the drug loaded nanoparticles were internalized in the cells. The blue fluorescence image shows emission from the nucleus stained with DAPI. The merged image of DOX and DAPI fluorescence (as is seen from the magenta colour) clearly indicates that DOX-PPMN is mainly localized in the cytoplasm. This study demonstrates that the use of these nanocarriers as drug delivery vehicles could significantly enhance the accumulation of the DOX at target cancer cells leading to a high therapeutic efficacy. Specifically, the present study demonstrates the formation of stable, highly crystalline, biocompatible, protein resistance polyphosphate grafted nanomagnets having good magnetization and excellent

intrinsic loss power. This makes it amenable for promising applications in hyperthermia treatment of cancer as well as pH triggered release of DOX for combination therapy involving hyperthermia and chemotherapy.

Conclusions

In summary, the synthesis of a hydrophilic multifunctional polyphosphate grafted nanomagnets of average size 10 nm is reported. XRD and TEM analysis confirmed the formation of highly crystalline single phase Fe₃O₄ nanostructures. The detailed structural analysis by FTIR, TGA, DLS and zeta-potential confirmed the successful grafting of nanomagnets with polyphosphate moieties. These superparamagnetic nanomagnets exhibit good colloidal stability and biocompatibility along with self-heating efficacy under AC magnetic field. The drug loading efficiency of the PPNM and their pH triggered release were also investigated by using DOX as a model drug. Cellular imaging experiments reveal that these nanomagnets can be easily internalized by cells. These multifunctional nanomagnets may have potential benefits by enhancement of *in-vivo* therapeutic efficacy *via* decreasing systemic toxicity of antitumor drugs both through protection of the drug throughout circulation and by means of magnetic fields to target the nanomagnets to the infected area. Further, high loading affinity for DOX with their sustained release and localized heating ability under AMF makes these novel magnetic nanoparticles suitable for cancer therapy.

Acknowledgements

Authors thank Dr. B. N. Jagatap, Director, Chemistry Group and Dr. V. K. Jain, Head, Chemistry Division, BARC for the encouragement and support. The authors also thank Dr. R. S. Ningthoujam, BARC for facilitating the use of the induction heater. Authors are grateful to Head, Analytical Chemistry Division, BARC for providing ICP-OES facility. The authors also thank Mr. Manjoor Ali and Ms. Vasumathy Pillai for confocal laser scanning microscopy studies.

Notes and references

1. J. Cheon and J. -H. Lee, *Acc. Chem. Res.*, 2008, **41**, 1630.
2. K. C. Barick, S. Singh, N. V. Jadav, D. Bahadur, B. N. Pandey and P. A. Hassan, *Adv. Funct. Mater.*, 2012, **22**, 4975.
3. O. D. Jayakumar, R. Ganguly, A. K. Tyagi, D. K. Chandrasekharan and K. Nair, *J. Nanosci. Nanotechnol.*, 2009, **9**, 6344.
4. J. Zhu, J. Wang, X. Wang, J. Zhu, Y. Yang, J. Tian, W. Cui, C. Ge, Y. Li, Y. Pan and H. Gu, *J. Mater. Chem. B*, 2015, **34**, 6905.
5. J. Zhu, B. Zhang, J. Tian, J. Wang, Y. Chong, X. Wang, Y. Deng, M. Tang, Y. Li, C. Ge, Y. Pan and H. Gu, *Nanoscale*, 2015, **7**, 3392.
6. C. Boyer, M. R. Whittaker, V. Bulmus, J. Liu and T. P. Davis, *NPG Asia Mater.*, 2010, **2**, 23.
7. J. Majeed, L. Pradhan, R. S. Ningthoujam, R. K. Vasta, D. Bahadur and A. K. Tyagi, *Coll. Surf. B*, 2014, **122**, 396.
8. Y. -K. Peng, C. N. P. Lui, T. -H. Lin, C. Chang, P. -T. Chou, K. K. L. Yung and S. C. E. Tsang, *Faraday Discuss.*, 2014, **175**, 13.
9. M. Das, D. Mishra, P. Dhak, S. Gupta, T. K. Maiti, A. Basak and P. Pramanik, *Small*, 2009, **5**, 2883.
10. D. Portet, B. Denizot, E. Rump, J. J. Lejeune and P. Jaller, *J. Coll. Interf. Sci.*, 2001, **238**, 37.
11. Y. Sahoo, H. Pizem, T. Fried, D. Golodnitsky, L. Burstein, C. N. Sukenik and G. Markovich, *Langmuir*, 2001, **17**, 7907.

12. S. Chandra, K. C. Barick and D. Bahadur, *Adv. Drug Del. Rev.*, 2011, **63**, 1267.
13. X. L. Liu, H. M. Fan, J. B. Yi, Y. Yang, E. S. G. Choo, J. M. Xue, D. D. Fan and J. Ding, *J. Mater. Chem.*, 2012, **22**, 8235.
14. J. Xie, K. Chen, H. Y. Lee, C. Xu, A. R. Hsu, S. Peng, X. Chen and S. Sun, *J. Am. Chem. Soc.*, 2008, **130**, 7542.
15. N. Bertrand, J. Wu, X. Xu, N. Kamaly and O. C. Farokhzad, *Adv. Drug Del. Rev.*, 2014, **66**, 2.
16. Z. Xiao, C. Ji, J. Shi, E. M. Pridgen, J. Frieder, J. Wu and O. C. Farokhzad, *Angew. Chem.*, 2012, **124**, 12023.
17. K. Yan, H. Li, P. Li, H. Zhu, J. Shen, C. Yi, S. Wu, K. W. Yeung, Z. Xu, H. Xu and P. K. Chu, *Biometer.*, 2014, **35**, 344.
18. C. Yee, G. Kataby, A. Ulman, T. Prozorov, H. White, A. King, M. Rafailovich, J. Sokolov and A. Gedanken, *Langmuir*, 1999, **15**, 7111.
19. P. Sharma, S. Rana, K. C. Barick, C. Kumar, H. G. Salunke and P. A. Hassan, *New J. Chem.*, 2014, **38**, 5500.
20. C. Tudisco, F. Bertani, M. T. Cambria, F. Sinatra, E. Fantechi, C. Innocenti, C. Sangregorio, E. Dalcanale and G. G. Condorelli, *Nanoscale*, 2013, **5**, 11438.
21. K. Löster, S. Seidel, D. Kirstein, F. Schneider and F. Noll, *J. Immunol. Methods*, 1992, **148**, 41.
22. R. Palmeira-de-Oliveira, A. Palmeira-de-Oliveira, C. Gaspar, S. Silvestre, J. Martinez-de-Oliveira, M. H. Amaral and L. Breitenfeld, *Int. J. Pharm.*, 2011, **421**, 130.
23. S. Vimal, S. A. Majeed, G. Taju, K. S. Nambi, N. S. Raj, N. Madan, M. A. Farook, T. Rajkumar, D. Gopinath and A. S. S. Hameed, *Acta Trop.*, 2013, **128**, 486.
24. K. Konecni, N. H. Low and M. T. Nickerson, *Food Chem.*, 2012, **134**, 1775.
25. S. Tripathy, S. Das, S. P. Chakraborty, S. K. Sahu, P. Pramanik and S. Roy, *Int. J. Pharm.*, 2012, **434**, 292.
26. N. N. Rao, M. R. Gómez-García and A. Kornberg, *Annu. Rev. Biochem.*, 2009, **78**, 605.
27. K. C. Barick and P. A. Hassan, *J. Coll. Interf. Sci.*, 2012, **369**, 96.
28. B. Ding, S. Xia, K. Hayat and X. Zhang, *Agric. Food Chem.*, 2009, **57**, 2938.
29. K. C. Barick, M. Aslam, Y. P. Lin, D. Bahadur, P. V. Prasad and V. P. Dravid, *J. Mater. Chem.*, 2009, **19**, 7023.
30. V. Zamora-Mora, M. Fernández-Gutiérrez, J. S. Román, G. Goya, R. Hernández and C. Mijangos, *Carbohydr. Polym.*, 2014, **102**, 691.
31. J. Wan, W. Cai, X. Meng and E. Liu, *Chem. Commun.*, 2007, 5004.
32. J. E. Wong, A. K. Gaharwar, D. Muller-Schulte, D. Bahadur and W. Richtering, *J. Nanosci. Nanotechnol.*, 2008, **8**, 4033.
33. M. Mikhaylova, D. Y. Kim, N. Bobrysheva, M. Osmolowsky, V. Semenov, T. Tsakalagos and M. Muhammed, *Langmuir*, 2004, **20**, 2472.
34. S. Chandra, S. Mehta, S. Nigam and D. Bahadur, *New J. Chem.*, 2010, **34**, 648.
35. L. S. Goldstein, M. W. Dewhirst, M. Repacholi and L. Kheifets, *Int. J. Hyperth.*, 2003, **19**, 373.
36. C. S. S. R. Kumar and F. Mohammad, *Adv. Drug Deliv. Rev.*, 2011, **63**, 789.
37. A. Tomitaka, T. Koshi, S. Hatsugai, T. Yamada and Y. Takemura, *J. Magn. Magn. Mater.*, 2011, **323**, 1398.
38. R. Ghosh, L. Pradhan, Y. P. Devi, S. S. Meena, R. Tewari, A. Kumar, S. Sharma, N. S. Gajbhiye, R. K. Vatsa, B. N. Pandey and R. S. Ningthoujam, *J. Mater. Chem.*, 2011, **21**, 13388.
39. M. Kallumadil, M. Tada, T. Nakagawa, M. Abe, P. Southern and Q. A. Pankhurst, *J. Magn. Magn. Mater.*, 2009, **321**, 1509.
40. S. Rana, N. V. Jadhav, K. C. Barick, B. N. Pandey and P. A. Hassan, *Dalton Trans.*, 2014, **43**, 12263.
41. S. Nigam, K. C. Barick and D. Bahadur, *J. Magn. Magn. Mater.*, 2011, **323**, 237.
42. E. Munnier, F. Tewes, S. Cohen-Jonathan, C. Linassier, L. Douziech-Eyrolles, H. Marchais, M. Soucé, K. Hervé, P. Dubois and I. Chourpa, *Chem. Pharm. Bull.*, 2007, **55**, 1006.
43. F. A. D. Wolf, K. Nicolay and B. D. Kruijff, *Biochem.*, 1992, **31**, 9252.
44. K. C. Barick, S. Nigam and D. Bahadur, *J. Mater. Chem.*, 2010, **20**, 6446.